Relationship between Kinetic and Thermodynamic Characteristics of Oxygen Dissociative Adsorption on Close-Packed Metal Surfaces

Ernst D. German* and Moshe Sheintuch

Department of Chemical Engineering, Technion-Israel Institute of Technology, Haifa 32000, Israel

Received: April 2, 2005; In Final Form: June 16, 2005

The activation energies and rate constants characterizing dissociative oxygen adsorption on transition and noble metal surfaces are calculated using a previously developed analytical formalism. Three approaches are considered: classical and quantum nonadiabatic approaches as well as a classical adiabatic approach. The results show a nonlinear relationship between the activation energies and the corresponding reaction energies. The effects due to the quantum description of the O−O bond and due to the Condon approximation are discussed. Calculated activation energies are compared with published experimental data.

1. Introduction

Oxygen dissociation on metal surfaces is an important step in catalytic oxidation reactions, and it frequently determines the direction and kinetics of the overall rate. Knowledge of the rate constant and/or the height of the activation barrier of this reaction is necessary to describe the whole multistep catalytic reaction. Predicting these reaction characteristics from data about oxygen molecule interaction with the metal will enable us to reduce (or even avoid) experimental work or laborious computations and will allow us to optimize the catalyst. The correlations between the activation energy (E_a) and reaction heat (ΔE) for gas-phase reactions or between E_a and the free energies of homogeneous catalytic reactions (Brønsted−Evans−Polanyi−Semenov relationship[1−10]) represent a dependency of similar kind and are considered to be a fundamental principle.

Recent works reported the relation between a calculated apparent activation energy ($E_a(\text{apparent}) = E_a - |\Delta E_i|$) and the corresponding heat ΔE_f (see Figure 5 of appendix C for notations) of N_2, CO, NO, or O_2 adsorption on flat and stepped surfaces.[11−14] On the basis of extensive, numerical (DFT) studies the authors found a linear relationship ($E_a(\text{apparent}) = 2.07 + 0.9\Delta E_f$ for close packed surfaces and $E_a(\text{apparent}) = 1.34 + 0.87\Delta E_f$ for stepped surfaces, energies in eV). The linear character of these relations was attributed to the fact that, for a given metal surface geometry, the transition state structures are essentially independent of the molecule and metal considered, and therefore, such linear relations were claimed to have a universal character. The free energy relations in heterogeneous catalysis and electrocatalysis were also considered in refs 15−17.

Recently, a simple analytical formalism was suggested[18−23] for describing the kinetics of dissociative adsorption of X_2 molecules. The rate constants in these works were calculated in terms of the classical[18] and quantum[23] approaches of the nonadiabatic method or by using the adiabatic potential energy surface (PES)[19−22] (we refer to these as approaches i, ii, and iii.) In contrast to laborious ab initio numerical calculations using high-dimensional PESs, three reaction coordinates are employed to construct the model PESs used in these three approaches: the distance x of X_2 molecular axis from a metal surface, the distance y between the X atoms, and the effective coordinate θ describing structure reorganization of metal atoms in the neighborhood of the adsorption site. The developed formalism does not require calculation of the whole potential surface and allows one to use the results of quantum chemical calculations for the initial and final states or the corresponding experimental data to calculate the transition state. Unlike published numerical calculations, the theory gives an analytical description of the relationship between the activation energy and reaction thermodynamics characteristics and, specifically, between the activation energy and the difference ($\Delta E = \Delta E_f - \Delta E_i$) of heats of the atomically (ΔE_f) and the molecularly (ΔE_i) adsorbed states. The theory also predicts a nonlinear dependence between E_a and ΔE. Although the quantitative difference between the nonlinear and linear description of E_a vs ΔE relationship may be small, particularly over a narrow domain of energies, it is of fundamental importance since the nonlinear dependence supports the used theoretical models.

A confirmation of the theoretical predictions have been obtained in ref 22 where the correlation between E_a and ΔE was studied for the dissociative oxygen adsorption on Rh(111), Ag(111), Ag(110), and Au(111) surfaces using approach (iii) only. An extension of the study to other metals (Ni, Cu, Pd, Pt, Ir, and Ru), that span a wider range of ΔE, and using the three approaches (i−iii) for each case, will render credibility to the theoretical conclusions, and this is the main goal of the present work. We apply all these approaches to calculate the activation energies and the rate constants for the dissociative oxygen adsorption on the transition metals listed above (the (111) metal surfaces of Ni, Cu, Pd, Pt, Ir, Ru, Rh, Ag, and Au as well as Ag(110)).

The other goal of the work is to compare the various models in order to estimate the role of quantum effects due to the O−O bond and the role of the Condon approximation on the activation characteristics of the oxygen dissociative adsorption.

The remainder of the paper is organized as follows. In section 2, the reaction model and the main theoretical approaches are described. The parameters used in the three approaches and the results of the calculations are given in section 3. Section 4 concludes the paper. Four appendices are supplied with the paper. Appendix A summarizes selected published data on oxygen molecular and atomic adsorption on transition metals. Computation details are presented in appendix B. The theoretical details are described in appendices C and D.

* To whom correspondence should be addressed. E-mail: ernst_german@yahoo.com.

10.1021/jp051678+ CCC: $30.25
Published on Web 08/13/2005

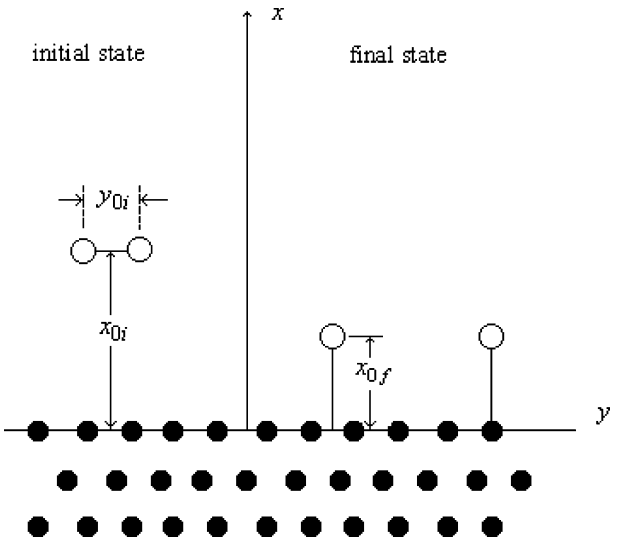

Figure 1. Equilibrium positions of adsorbed oxygen molecule and oxygen atoms on a metal surface.

2. Model and Theoretical Approaches

A generally accepted view[14,24] of the mechanism of dissociative adsorption of an O_2 molecule on transition metals is that of a two-step process. The first step is the nonactivated formation of a stable, molecularly adsorbed complex (precursor) between O_2 and a metal surface

$$O_2 + \text{metal} \leftrightarrow O_2\text{*/metal} \qquad \text{(I)}$$

where an "asterisk" denotes that the O−O bond is somewhat stretched compared to that in a free molecule, due to a partial charge transfer from the metal to the molecule. The second step is the activated transition of the precursor to the atomic adsorbed (final) state when the O−O bond is disrupted, and the O atoms approach closer to the metal surface

$$O_2\text{*/metal} \rightarrow (O\cdots O)\text{/metal} \qquad \text{(II)}$$

In this paper we consider only reaction II, for which the rate constant of formation of the dissociated state (O···O)/metal from the precursor O_2*/metal is calculated. This reaction is the rate-determining step of the above mechanism since step I is believed to be nonactivated.

The detailed descriptions of the approaches used here have been published elsewhere;[18−20] a short review follows. The O_2 molecule is assumed to be in a position parallel to the metal (Figure 1). The initial, U_i, and final, U_f, PESs are introduced to describe step II. Each of these potential surfaces represents the total energy of the whole system that depends on a set of coordinates $\{r_k\}$ describing the vibrations of the metal nuclei, on the distance x between the center of mass of O_2 and the metal surface, and on the distance y between oxygen atoms. The symbol O_2 is used here as a general notation of the reactant in the undissociated and dissociated state. The simplest form of U_i and U_f is that obtained under the assumption that the vibration modes along the coordinates x, y, and $\{r_k\}$ are not coupled. In this case, both potential surfaces may be written as a sum of three separate components: $\upsilon(x)$ which characterizes the interaction between O_2 and a metal surface in the direction perpendicular to the surface (Figure 5 and eqs C1 and C2 of appendix C), $u(y)$ which is the vibration potential for O_2 (Figure 6 and eqs C4 and C6 of appendix C), and $w(\{r_k\})$ which describes the vibrations of the metal atoms (Figure 6 of appendix C). Thus, providing these components with the subscripts "i" and "f", we write these PESs in the following form[18]

$$U_i(x,y,\{r_k\}) = w_i(\{r_k\}) + u_i(y) + \upsilon_i(x) \qquad (1')$$

$$U_f(x,y,\{r_k\}) = w_f(\{r_k\}) + u_f(y) + \upsilon_f(x) + \Delta E \qquad (1'')$$

where ΔE is the difference of the energy values at the minima of the potential energy surfaces of the final and initial states; the minimum energy of the initial state is taken to be zero.

Nonadiabatic Approaches. Using the nonadiabatic approach for the calculation of the dissociative adsorption kinetics is, strictly speaking, justified if only the resonance interaction between a molecule and a metal surface at the reaction distances, $V(\hat{x},\hat{y})$, is lower than k_BT. However, the nonadiabatic approach proves to be useful even if the adiabaticity criterion is not fulfilled: the adiabatic case results may be obtained from the nonadiabatic one by correcting the activation energy using the approximate expression (see ref 25). The classical limit calculations of the activation energies of dissociative oxygen adsorption (Table 1) performed in this work demonstrate that the adiabatic values are really close to the "corrected" nonadiabatic energies (see section 3.2). In terms of nonadiabatic approaches, the rate constant (W) is calculated as the average probability of the transition per unit time from the initial PES U_i (molecularly adsorbed state) to the final PES U_f (atomically adsorbed state). The calculations are performed using both a classical approximation and quantum mechanical description.

(i) Classical Approximation.[18] The most appropriate method for this purpose is the *Fermi golden rule*. The calculations lead to the following equation for the rate constant of the nonadiabatic reaction

$$W_{cl}^{na} = \frac{(2\pi)^{3/2}(k_BT)^{1/2}V^2}{\hbar Z_x Z_y \sqrt{|\Gamma(\hat{x},\hat{y},\hat{\theta})|}} e^{-E_{a,cl}^{na}/k_BT} \qquad (2)$$

where the activation energy is equal to

$$E_{a,cl}^{na} = \upsilon_i(\hat{x}) + u_i(\hat{y}) + \hat{\theta}^2 E_r = \upsilon_i(\hat{x}) + u_i(\hat{y}) + \frac{[\Delta E + \upsilon_f(\hat{x}) + u_f(\hat{y}) - \upsilon_i(\hat{x}) - u_i(\hat{y}) + E_r]^2}{4E_r} \qquad (3)$$

In eqs 2 and 3, V is the effective electron matrix element which is of the order k_BT or smaller, Z_x and Z_y are the partition functions, and E_r is the reorganization energy.[18] θ is the effective coordinate which may be introduced (in harmonic approximation) instead of the set of the coordinates $\{r_k\}$ for describing the movement of the system over the coordinates $\{r_k\}$ along the potential surfaces U_i and U_f. The "cap" over x, y, and θ denotes that these coordinates are taken at the saddle point that is determined by a set of three equations. The quantity Γ may be represented as a combination of the first and the second derivatives of the function υ and u over x and y, of the θ coordinate, and of the reorganization energy.[26]

(ii) Quantum Mechanical Description.[23] In contrast to the previous approach, in this model the motion along the y-coordinate (i.e., O−O vibration) is considered as having quantum character. It physically means that the transition along this coordinate proceeds by tunneling from the ground and some excited O−O vibration levels ν in the initial potential, $u_i(y)$, of the molecularly adsorbed oxygen into the a continuous manifold of energies in the final decaying potential, $u_f(y)$, under

TABLE 1: Comparison of the Classical Nonadiabatic and Adiabatic Activation Energies and Rate Constants[a]

		nonadiabatic model			adiabatic model		
metal	ΔE	E_a^{na}	$E_a^{ad,approx}$	$\log k_{298}^{approx}$	E_a^{ad} true	E_a^{ad} apparent	$\log k_{298}$ true
1 Ni(111)	−88	0.85	−0.24	13.13	0	−17	12.65
2 Cu(111)	−73	3.60	2.54	10.49	2.56	−10.4	10.62
3 Rh(111)	−61	3.50	2.23	10.78	2.25	−21.8	11.09
4 Ir(111)	−57.1	5.13	3.71	9.59	3.73	−4.17	10.0
5 Ru(111)	−46.4	9.80	8.29	6.23	8.29	−25.3	6.66
6 Pd(111)	−45.5	7.52	6.10	7.91	6.11	−2.4	8.24
7 Pt(111)	−39.5	11.92	10.51	4.63	10.51	2.0	5.00
8 Ag(110)	−32.0	13.78	12.60	3.23	12.69	3.0	3.33
9 Ag(111)	−19.5	20.77	19.26	−1.86	19.26	8.7	−1.37
10 Au(111)	12	44.0	42.59	−19.14	42.60	37.6	−18.40

[a] $\Delta E = \Delta E_f - \Delta E_i$, energies in kcal/mol, rate constants in s^{-1}; $E_a^{ad,approx} = E_a^{na} - 2V_{tr}^{na}(\hat{\theta}(1-\hat{\theta}))^{1/2}$ [25] where $V_{tr}^{na} = V_{0e}{}^{-(\hat{x}-x_{0i})}(1-\epsilon e^{-(\hat{y}-y_{0i})})$ (see appendix C).

conditions of the Franck−Condon principle. The equation for the rate constant obtained in the quantum model (for details, see ref 23) has the form

$$W = \sum_{\nu=0} A_\nu e^{-\sigma(\nu,\hat{x}^*)} \exp\left[-\frac{E_a^\nu(\hat{x}^*)}{k_B/T}\right] \equiv A_{qu}^{na} \exp\left[-\frac{E_{a,qu}^{na}}{k_B/T}\right] \quad (4)$$

where

$$E_a{}^\nu(\hat{x}^*) = \epsilon_i{}^0 - \epsilon_i{}^\nu + \upsilon_i(\hat{x}^*) + \hat{\theta}^2 E_r$$

Here $\sigma(\nu)$ is the quantity characterizing tunneling from the quantum energy level $E_i{}^\nu$ of the initial potential $u_i(y)$, $\epsilon_i{}^0$ is the zero-point vibration level, and $\hat{x}$ denotes the value of this coordinate at the transition state for an arbitrary mutual disposition of the curves u_i and u_f; an "asterisk" at $\hat{x}$ means that the value of $\hat{x}^*$ corresponds to the optimum disposition of these curves. The effective activation energy $E_{a,qu}{}^{na}$ and the preexponential $A_{qu}{}^{na}$ are then determined numerically as $d \ln W/d(1/T)$ (the preexponential $A_{qu}{}^{na}$ includes the tunneling factor).

(iii) Adiabatic Approach, Classical Approximation.[19−22] According to this approach, the coordinates of the saddle point on the adiabatic PES determine the activation barrier of the dissociative adsorption in the classical limit. The adiabatic PES U is constructed from the diabatic PESs U_i and U_f of the above model (i) by a usual way

$$U = 1/2\lfloor U_i + U_f - ((U_i - U_f)^2 + 4V^2)^{1/2}\rfloor \quad (5)$$

The saddle point coordinates, $\hat{x}$, $\hat{y}$, and $\hat{\theta}$, are calculated by solving a set of equations similar to that for the model (i) in which, however, the dependence of the half-splitting V on coordinates x and y is taken into account (without use of a non-Condon approximation). These coordinates when substituted into the equation for U lead to the activation energy equal to

$$E_{a,cl}^{ad} = U_i(\hat{x},\hat{y},\theta) - \frac{V(\hat{x},\hat{y})}{\sqrt{(1-\hat{\theta})/\hat{\theta}}} = \upsilon_i(\hat{x}) + u_i(\hat{y}) + \hat{\theta}^2 E_r - \frac{V(\hat{x},\hat{y})}{\sqrt{(1-\hat{\theta})/\hat{\theta}}} \quad (6)$$

In the adiabatic model, the rate constant is calculated by the standard equation

$$W_{cl}^{ad} = \frac{k_B T}{h}\frac{\hat{Z}'}{Z_i} \exp[-E_{a,cl}^{ad}/k_B T] \equiv A^{ad} \exp[-E_{a,cl}^{ad}/k_B T] \quad (7)$$

where Z_i is the partition sum of the initial (molecularly adsorbed) state and $\hat{Z}'$ is that of the transition state.

3. Discussion

3.1. Parameters of Equations. To locate the transition state in terms of the above approaches, one needs to specify the structures of the initial (molecularly adsorbed) and the final (dissociated) equilibrium states of an oxygen molecule on a metal surface (111). This implies knowledge of characteristics of both the interaction of the oxygen molecule or atoms with the metal surface and the mutual interaction of oxygen atoms (see appendix A, Tables 3−8). These adsorption characteristics are indeed parameters of the equations determining the saddle point coordinates.[18−23] The *bond-hole-top* structure is considered as the *initial* state for the systems described here, while the *atom-hole* structure is considered for the *dissociated* oxygen atoms; these are energetically more favorable than other molecular and atomic adsorbed structures (see for example ref 27). The required parameters may be extracted from experimental data, obtained from quantum chemical calculations, or estimated from a similarity between the considered system and a system the parameters of which are known.

These parameters may be formally divided in three groups. One group characterizes mainly the adsorbed oxygen molecule at a large distance of a metal surface. The corresponding parameters are the O−O bond length y_{0i}, the O−O vibration frequency $\omega_i{}^y$, and the dissociation energy B_i of the O−O interaction potential and the preexponential factor $B_f{}^e$ (see appendix C). These quantities may be approximately assumed constants for all considered metals. The y_{0i} and $\omega_i{}^y$ values may be set equal to 1.4 Å and 850 cm^{-1}, respectively, according to the data in Tables 3−8. The values of $B_i = 80$ kcal/mol and $B_f{}^e = 0.3B$ (appendix C) are considered to be constant for all the metals.

The second group of parameters characterizes the interaction of the oxygen molecule and atoms with a metal surface. Some of these are weakly dependent on the metal nature while others depend strongly on the metal nature (Tables 3−8). Fortunately, the adsorption heights and frequencies (shown in the tables) are usually well predicted by quantum chemical methods (periodic DFT and cluster models); similar values are obtained either from experimental data or from results of various computation methods. We chose to use, in this work, the parameter values obtained by the cluster model (appendix A, Table 9). However, the quantum chemical methods are not very successful in describing the adsorption heats ΔE_i and ΔE_f as can bee seen from Tables 3−8. Therefore, it seems reasonable to use the experimental data (when available) to calculate the transition states in terms of our theory. Experimental values for

TABLE 2: Comparison of the Nonadiabatic Classical and Quantum Activation Energies and Rate Constants[a]

		classical model		quantum model	
metal	ΔE	E_a^{na}	$\log k_{298}/s^{-1}$	E_a^{na}	$\log k_{298}/s^{-1}$
1 Ni(111)	−88	0.85	12.50		
2 Cu(111)	−73	3.60	9.71	2.15	10.17
3 Rh(111)	−61	3.50	9.84	1.72	10.10
4 Ir(111)	−57	5.13	8.56	2.99	9.72
5 Ru(111)	−46.4	9.80	5.11	7.13	6.61
6 Pd(111)	−45.5	7.52	6.88	4.97	8.37
7 Pt(111)	−39.5	11.92	3.60	9.04	5.17
8 Ag(110)	−32	13.78	2.36	10.89	3.77
9 Ag(111)	−19.5	20.77	−2.97	17.9	−1.22
10 Au(111)	12	44.0	−20.18		

[a] Energies in kcal/mol.

the adsorption heats, ΔE_f, were used for all systems considered here, but the measured ΔE_i values were available only for the Pt(111)/O_2 and Pd(111)/O_2 systems (as well as for the noble metals to which we refer in this work or as well as for the noble metals considered in ref 22). Therefore calculated values of ΔE_i were used for the remaining systems. Since the adsorption heats, ΔE_i, change within a rather small range, as compared to that for ΔE_f, an inaccuracy in these calculations will not be of important significance.

The last parameter we consider here is the metal reorganization energy E_r, characterizing the local change of a metal structure near the adsorption center (appendix D). The value of E_r was estimated from the six atoms (M_6) cluster model using the changes of the cluster bond lengths M−M under formation of the dissociated oxygen state (Figure 4a) from the molecularly adsorbed state (Figure 4b). Estimated values of the reorganization energies are equal to about 4 kcal/mol for the Pd(111), 21 kcal/mol for the Ni(111), and 25 kcal/mol for the Cu(111). We were not able to accurately estimate the changes of the M−M bond for the Ir(111), Pt(111), and Ru(111) clusters; therefore, the reorganization energy for these metals was intuitively taken as that for palladium and for noble metals.[18] Although this choice does not have a rigorous quantitative basis, it should provide a plausible initial step for studying the correlation relations. One should note that according to our estimations, inaccuracy of E_r in the range of ±30% will affect the activation energy for these systems by only ca. ±0.6 kcal/mol.

The adsorption characteristics for nickel, copper, platinum, palladium, iridium, and ruthenium used in our calculations are listed in Table 9 along with the corresponding data for other metals taken from ref 22; experimental values of adsorption heats are denoted by bold characters.

3.2. Results. Tables 1 and 2 present the results of calculations using approaches i−iii described above. In Table 1, the activation energies and the corresponding rate constants calculated by the adiabatic approach (iii) are compared with those calculated by the nonadiabatic approach (i). The values of the E_a^{na} are greater than those of E_a^{ad} by a value corresponding to the splitting of the diabatic terms in the transition state (Figure 5). The interesting result is that the approximate activation energies $E_a^{ad,approx}$, estimated from the nonadiabatic energies using the approximate equation of ref 25 $E_a^{ad,approx} = E_a^{na} - 2V_{tr}^{na}(\hat{\theta}(1-\hat{\theta}))^{1/2}$ (where V_{tr}^{na} is given by eq C11), coincide exactly with the adiabatic energies. It implies that the coordinates of the transition states $\hat{x}$, $\hat{y}$, and $\hat{\theta}$ calculated in both of these models are very close to each other. This fact justifies the use of both the nonadiabatic models for studying the oxygen adsorption kinetics (see text after eqs 1′ and 1″), which allows

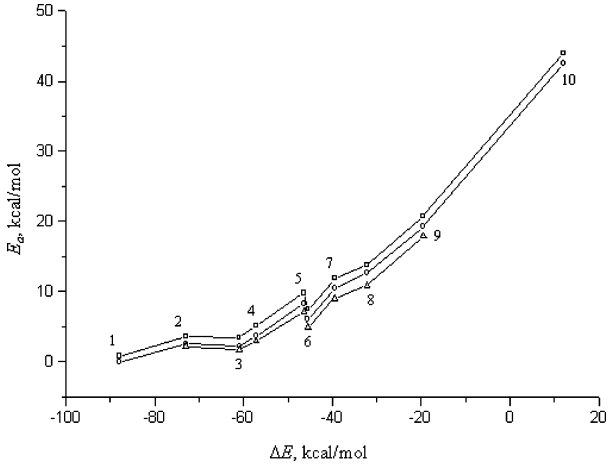

Figure 2. Activation energies calculated by the nonadiabatic and adiabatic approaches vs the reaction heat ΔE: quadratic, circles, and triangle symbols refer to models i, ii, and iii, respectively. The numeration of points corresponds to the metals listed in Tables 1 and 2.

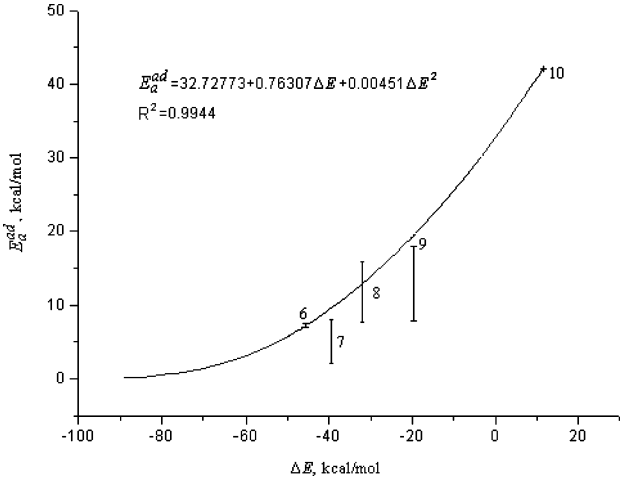

Figure 3. Quadratic approximation of the correlation between the true adiabatic activation energies and the reaction heats ΔE. Bars denote values of experimental intervals of the activation energies; the metals are numbered as in Tables 1 or 2.

the calculation of the preexponential factor of the rate constant in terms of a simpler procedure rather than that using the adiabatic approach. Comparison of the classical (i) and the quantum (ii) nonadiabatic models (Table 2) shows that accounting for quantum effects leads to a decline of the activation barrier of a rate constant, and this decline is smaller for the more exothermic reactions (Cu(111)/O_2) than for the system characterized by a lower negative ΔE (Ag(111)/O_2). Thus, the tunneling along the *y*-coordinate is more important for the second system than that for the last one.

The activation energies calculated by approaches i−iii (Tables 1 and 2) show a nonlinear dependence on the reaction energies ΔE (Figure 2). This is even more evident in Figure 3 where the dependence of the adiabatic activation energies E_a^{ad} on ΔE in a wide range of the reaction heats is well approximated by a quadratic function (correlation coefficient $R^2 = 0.994$). The change in ΔE is mainly due to the change of the binding energy for the dissociated state, ΔE_f, since the adsorption heats of the molecularly adsorbed state, ΔE_i, change in a rather narrow range of values (between −7 kcal/mol for Au(111) and −16.5 kcal/mol for Ni(111)), $\Delta E_i = -33.6$ kcal/mol for Ru(111) is exceptional). This leads also to the quadratic relation between

TABLE 3: Experimental Adsorption Data and Results of Theoretical Calculations Modeling the "Hole" Oxygen Adsorption on a Pd(111) Surface[a]

x_{0i}	y_{0i}	ω_i^x	ω_i^y	ΔE_i	x_{0f}	ω_f^x	ΔE_f	E_a	refs and comments
				−7.6 to −9.1			−53; −55		experiment TPD[37, 38]
			850			485		7 to 7.5	experiment EELS[39, 40, 41]
								20	periodic DFT[b]; $\chi = {}^1/_2$ mL[42]
1.75	1.39	390	890	−23.1	1.19	490	−43	25.6	periodic DFT[c]; $\chi = {}^1/_2$ mL[27,43]
1.67		450[d]		−8.1	1.138	498	−42.3		DFT; cluster model; this work[e]

[a] Distances x_{0i}, y_{0i} and x_{0f} in angstroms (see Figure 1), frequencies in cm^{-1}, heats of the molecular (ΔE_i) and dissociative (atomic) (ΔE_f) adsorption in kcal/mol, χ is the surface coverage. [b] This value of E_a characterizes the reaction path involving formation of the *top−fcc−bond* precursor. [c] The data correspond to the reaction path involving formation of *top−fcc−bond* precursor. [d] Average value of the frequencies Pd−O and Pd_2−O. [e] The calculated values of the parameters refer to the triplet electronic state of the palladium complexes; x_{0f} and ω_f^x were calculated on the model complex Pd_6O; other characteristics in the row were calculated on the model complex Pd_6O_2.

the apparent activation energies E_a^{ad}(apparent) $= E_a^{ad} - |\Delta E_i|$ and the energies ΔE_f ($R^2 = 0.965$). This result is different from that of refs 7−10 to which we referred in the Introduction where the linear relationship between the apparent activation energies and ΔE_f is supposed to have a universal character. The nonlinear character of the above relationships may be induced particularly from eq 3: The activation energy depends explicitly on ΔE^2 and implicitly on the saddle point coordinates $\hat{x}$, $\hat{y}$, and $\hat{\theta}$, which in turn depend implicitly on ΔE also (see also appendix C, eqs C1, C2, C4, and C6).

We compare now the *true* activation energies calculated via approaches i−iii with the corresponding experimental data. To the best of our knowledge the experimental values were measured for oxygen dissociative adsorption on palladium (number 6 in Tables 1 and 2), platinum (7), and on other noble metals (8 to 10). The experimental activation energy for palladium was reported to be 7 to 7.5 kcal/mol (Table 3), which is quite close to our estimations, 5 to 7.5 kcal/mol (Tables 1 and 2). The value obtained by the periodic DFT method leads to 20 to 26 kcal/mol. The experimental value for Pt(111) is in the range of 2 to 8 kcal/mol (Table 5) vs the calculated 9 to 12 kcal/mol (Tables 1 and 2). The value obtained by periodic DFT method is equal to 19.8 kcal/mol.

Comparison of the true activation energies of the dissociative oxygen adsorption on noble metals calculated via approach iii with the corresponding experimental data has been done in ref 22. Taking into account the calculations performed in this work by methods i and ii (Tables 1 and 2), we estimate the following ranges for the activation energies: 11 to 14 kcal/mol for Ag(110), 18 to 21 kcal/mol for Ag(111), and 42.5 to 44 kcal/mol for Au(111) (the corresponding experimental values cited in ref 22 are 8 to 16 ± 7 kcal/mol for Ag(110), 8 to 18 kcal/mol for Ag(111), and 42 kcal/mol for Au(111), respectively). The pictorial comparison of the theory with the available experimental data (for Pd, Pt, and noble metals) is also shown in Figure 3 where the intervals of experimental activation energies are presented.

The predicted *apparent* activation barriers for dissociation lie below the vacuum level for all studied transition metals except for platinum (Table 1). Our estimation of the apparent E_a for Pt(111), based on parameters values of the of Table 9, leads to a value (2 kcal/mol) which is above the vacuum level and that is in contrast to the negative experimental value of about −1.5 kcal/mol. This disagreement can be considered mainly due to the slightly overestimated adsorption height x_{0i} calculated by periodic DFT in ref 43; using the $x_{0i} = 1.75$ Å value (instead of $x_{0i} = 1.78$ Å in Table 9) leads to the negative apparent activation energy of ca. −0.2 kcal/mol.

Before concluding, we will discuss the effect of the oxygen coverage on the dissociation activation barrier. That dependence may be simply obtained from eq 3, which includes the reaction heat ΔE as a parameter. The reaction heat, being negative for all metals except Au(111), is sensitively dependent on oxygen coverage. For example, if ΔE varies linearly with coverage (χ), that is, $\Delta E = \Delta E_0 + C\chi$, then eq 3 predicts the following approximate coverage dependence of the activation energy

$$E_{a,cl}^{na}(\chi) = E_{a,cl}^{na}(0) + k_1\chi + k_2\chi^2 \qquad (8)$$

where the coefficients k_1 and k_2 are expressed by the terms of eq 3. For example, according to ref 58 of Table 5, the coefficient C for the oxygen adsorption on Pt(111) may be estimated to be equal to 32 (kcal/mol)/mL for the range of coverage of χ from 0 to 0.25 mL. The use of this value of C leads to the values of k_1 and k_2 equal to 16 and 64 (kcal/mol)/mL, respectively (for this coverage interval).

4. Conclusions

A nonlinear relationship between the activation energies and the reaction heats of oxygen dissociative adsorption on transition and noble metals was derived by the analytical formalism for the dissociative adsorption of X_2 molecules on metal surfaces, which is corroborated by numerical calculations for oxygen molecule and by published experimental data. It was shown that the nonadiabatic and adiabatic approaches lead to similar structures of the corresponding transition states. Accounting for the quantum character of the O−O vibration yields lower activation barriers than the classical approach, and the effect is greater, as the reaction is less exothermic. The coverage dependence of the calculated activation energy was described.

Appendix

A. Summary of Physical Characteristics of Oxygen Molecular and Atomic Adsorption. In this appendix, we compile (in Tables 3−9) the physical characteristics of oxygen adsorption on metal surfaces using published data as well as data calculated in the present work using the simple M_6 cluster model (Figure 4; for details of the calculations, see appendix B).

B. Computation Details. DFT as implemented in Gaussian98[28] has been used for all calculations. We employed the B3LYP functional, which uses a combination of Becke-3 (B3)[29] exchange functional and Lee−Yang−Parr (LYP) correlation functional.[30] The basis set used for the Pd atom is LANL set for the effective core potentials of double-ζ type (LANL2DZ),[31] which provides good physical characteristics for Pd clusters.[32−34] For oxygen, the basis set aug-cc-pVDZ[35] including polarization and diffuse functions was used to take into account a possible charge transfer to the adsorbate molecule used.

The calculations on the cluster model depend on the spin state of the cluster employed. Therefore, the energetic calculations

TABLE 4: Experimental Adsorption Data and Results of Theoretical Calculations Modeling the "Hole" Oxygen Adsorption on a Ni(111) Surface[a]

x_{0i}	y_{0i}	ω_f^x	ΔE_i	x_{0f}	ω_f^x	ΔE_f	E_a	refs and comments
				1.16 ± 0.08[b]				NEXAFS[44]
				1.11 ± 0.06				LEED[45]
						−105		calorimetry[46]
				1.08 ± 0.02				NEXAFS[47]
				1.21 ± 0.09				LEED[48]
				1.14		−97.8		periodic DFT; $\chi = {}^1/_3$ mL[49]
								periodic DFT[27,43 c]
				1.16		−107		$\chi = {}^1/_4$ mL
1.62	1.47		−38	1.12		−97.6	5.1	$\chi = {}^1/_2$ mL
1.689		476[d]	−16.5	1.200	566	−88		DFT; cluster model; this work[e]

[a] See footnote a to Table 1. [b] Evaluated using the distance a(Ni−Ni) = 2.49 and l(O−Ni) = 1.85 Å for 3-fold coordinated adsorption site. [c] The data refer to the reaction path involving formation of the *top−fcc−bond* precursor. [d] Average value of the frequencies Ni−O and Ni_2−O. [e] x_{0i}, ω_f^x, and ΔE_i were calculated on the Ni_6O_2 molecular complex (Figure 4a), x_{0f} and ω_i^x were calculated on Ni_6O atomic complex (Figure 4c), both in the septet electronic state, and ΔE_f was calculated on Ni_6O_2 in the quintet electronic state.

TABLE 5: Experimental Adsorption Data and Results of Theoretical Calculations Modeling the "Hole" Oxygen Adsorption on a Pt(111) Surface[a]

x_{0i}	y_{0i}	ω_i^x	ω_i^y	ΔE_i	x_{0f}	ω_f^x	ΔE_f	E_a	refs and comments
									AES,EELS,UPS,TDS,LEED[50,51]
		390	870	−8.8		490	−47.8	∼8	$\chi \sim$ mL
				−3.8					$\chi = {}^1/_4$ mL
				−8.4			−48	∼2	TDS, LEED[52], $\chi \sim 0$ mL
		380	875			480			EELS, LEED, TDS[53,54]
					1.18				LEED[55]
							−73		calorimetry [56] $\chi = 0$ mL
							−50		$\chi \sim 0.6$ mL
	1.32 ± 0.05								near-edge X-ray[57]
									AES, LEED, UPS, HREELS, TPD[58]
						466	−51		$\chi = 0$ mL
							−43		$\chi = {}^1/_4$ mL
	1.37 ± 0.05								NEXAFS[59]
									scattering of molecular beams[60]
							−50.9	−1.5[b]	low coverage
							−41		near saturation
	1.37								X-ray photoemission spectra[61]
	1.43								
		380	855			475			HREELS, TDP[62]
1.78	1.43	340	690	−15.6	1.23	470	−38	19.8	periodic DFT[27,43 c]
						510	−32		DFT; cluster model; fixed Pt−Pt[63]
					1.240	484			DFT; cluster model; Pt_3[64]
					1.237				DFT; cluster model; this work[d]

[a] See footnote a to Table 1. [b] Apparent activation energy. [c] For the *top−fcc−bond* precursor state. [d] Quintet electronic state.

TABLE 6: Experimental Adsorption Data and Results of Theoretical Calculations Modeling the "Hole" Oxygen Adsorption on a Cu(111) Surface[a]

x_{0i}	y_{0i}	ω_i^x	ω_i^y	ΔE_i	x_{0f}	ω_f^x	ΔE_f	E_a	refs and comments
		330	850			380			HREELS[65]
					1.1				SEXAFS[66]; fixed Cu−Cu
					0.2 ± 0.2				relaxed Cu−Cu
								2−4[c]	LEED-AES[67]
						403			EELS[68]
							−86.2		microcalorimetry[69]
							−81.2		DFT, cluster model[70]
					1.35		−81.6		Cluster model[71]
1.55[b]	1.48[b]		729[b]	−12.7[b]	1.13	482	−74	5	Periodic DFT; $\chi = {}^1/_4$ mL[72]
					1.23				DFT; cluster model; two layers [73]
1.901		229		−13[c]	1.261	461	−77.7		DFT; cluster model; this work[d]

[a] See footnote a to Table 1. [b] For the *bond−hole−bond* precursor state. [c] Apparent activation energy. [d] x_{0i}, ω_i^x, and ΔE_i were calculated on the Cu_6O_2 molecular complex (Figure 4a), and ΔE_f was calculated on Cu_6O_2 dissociated complex (Figure 4b), both in singlet electronic state; x_{0f} and ω_f^x were calculated on Cu_6O atomic complex in triplet electronic state (Figure 4c).

were performed for a number of the multiplicities of the M_6 clusters and the M_6/oxygen complexes. The results presented in Tables 3−9 correspond to the multiplicities of the lower electronic state (see footnotes to Tables).

The heats of the molecular and atomic adsorption, ΔE_i and ΔE_f, are calculated as the difference $\Delta E_{i(f)} = E_{i(f)} - E_\infty(M_6/O_2)$, where E_i and E_f are the total energies of the precursor and the dissociated state and E_∞ is the energy of the system M_6/O_2

TABLE 7: Experimental Adsorption Data and Results of Theoretical Calculations Modeling the "Hole" Oxygen Adsorption on an Ir(111) Surface[a]

x_{0i}	y_{0i}	ω_i^x	ω_i^y	ΔE_i	x_{0f}	ω_f^x	ΔE_f	E_a	refs and comments
			740			550			EELS[74]
			805						EELS[75]
							-65 ± 3		LEED, Auger; $\chi \sim 0$[76]
1.75	1.48			-26	1.31	504	-65.7	1.4	periodic DFT; $\chi = {}^1/_4$ mL ;fixed Ir−Ir[77]
1.715		450		-7.9	1.244	630	-76.2		DFT; cluster model; this work[b]

[a] See footnote a in Table 1. [b] x_{0i}, ω_i^x, and ΔE_i were calculated on the Ir_6O_2 molecular complex (Figure 4a), and ΔE_f was calculated on Ir_6O_2 dissociated complex (Figure 4b), both in triplet electronic state; x_{0f} and ω_f^x were calculated on Ir_6O atomic complex in triplet electronic state (Figure 4c).

TABLE 8: Experimental Adsorption Data and Results of Theoretical Calculations Modeling the "Hole" Oxygen Adsorption on a Ru(111) Surface[a]

x_{0i}	y_{0i}	ω_i^x	ω_y^x	ΔE_i	x_{0f}	ω_i^f	ΔE_f	refs and comments
							-80	LEED,AES[78]
				-5 to -22			-107	TPD[79, b]
1.758		496		-33.6	1.278	612	-105	DFT; this work; cluster model[c]

[a] See ref a to Table 1. [b] Polycrystalline; [c] x_{0i}, ω_i^x, and ΔE_i were calculated on the Ir_6O_2 molecular complex (Figure 4a), and ΔE_f was calculated on Ir_6O_2 dissociated complex (Figure 4b), both in quintet electronic state; x_{0f} and ω_f^x were calculated on Ir_6O atomic complex in triplet electronic state (Figure 4c).

TABLE 9: Parameters Used to Calculate the Transition Configurations[a]

	1 Ni(111)	2 Cu(111)	3 Rh(111)	4 Ir(111)	5 Ru(111)	6 Pd(111)	7 Pt(111)	8 Ag(110)	9 Ag(111)	10 Au(111)
x_{0i}	1.689	1.901	1.696	1.715	1.578	1.67	1.78	0.97	1.67	1.78
ω_i^x	476	229	409	450	496	450	380	250	450	380
ΔE_i	-17	-13	**-24**	-7.9	-33.6	**-8.5**	**-8.5**	**-9.7**	**-10.6**	**-5**
x_{0f}	1.20	1.26	1.191	1.244	1.278	1.138	1.18	0.104	1.138	1.18
ω_f^x	566	461	572	630	612	498	480	317	498	480
ΔE_f	**-105**	**-86**	**-85**	**-65**	**-80**	**-54**	**-48**	**-41.7**	**-30.1**	**7**

[a] Distances x_{0i}, y_{0i}, and x_{0f} in angstroms, frequencies in cm^{-1}, heats of the molecular (ΔE_i) and dissociative (ΔE_f) adsorption in kcal/mol; experimental adsorption heats are denoted by bold characters.

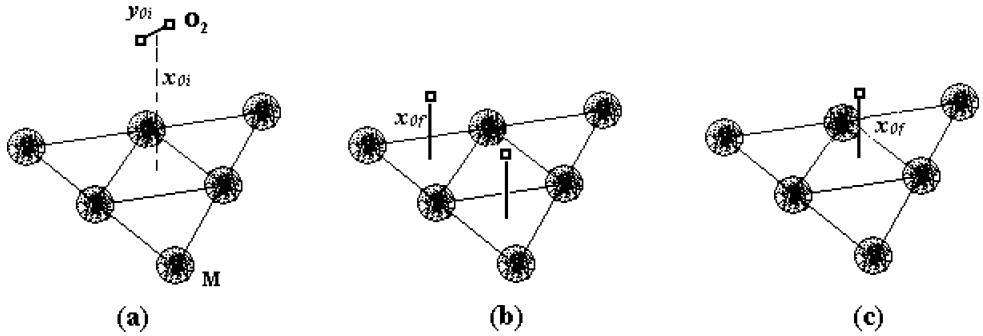

Figure 4. Structure of the metal/oxygen complexes used for the calculation of the corresponding adsorption characteristics: (a) molecular adsorption, (b) dissociative adsorption, and (c) adsorption of a single oxygen atom. All M−M bonds are taken to be equal to each other; x_{0i} is the distance of an oxygen from a surface, y_{0i} is the distance between O atoms in the molecular adsorbed state, and x_{0f} is the distance of an oxygen atom from a surface in the final (dissociated) state.

at a large distance (15−20 Å) that practically corresponds to the independent components M_6 and O_2.

C. Interaction Potentials and the Effective Resonance Integral. The interactions of oxygen molecule and atoms with the "holes" of the metal surface (111) (which are the components of eq 1) are approximated by the following Morse functions[18−23] (Figure 5)

$$v_i(x) = D_i[1 - e^{-\beta_i(x-x_{0i})}]^2 \quad \text{(C1)}$$

$$v_f(x) = D_f[1 - e^{-\beta_f(x-x_{0f})}]^2 \quad \text{(C2)}$$

where x is the distance between the center of mass of the dioxygen and the surface and

$$\beta_{i(f)} = \omega_{i(f)}{}^x \sqrt{M/2D_{i(f)}} \quad \text{(C3)}$$

In eq C3, M is approximately the mass of the dioxygen, and ω_i^x and ω_f^x are the vibration frequencies of the oxygen molecule and oxygen atoms relative to the metal surface.

The potential energy of the oxygen molecule in the precursor state is represented by the Morse function of the interatomic distance y (Figure 6)

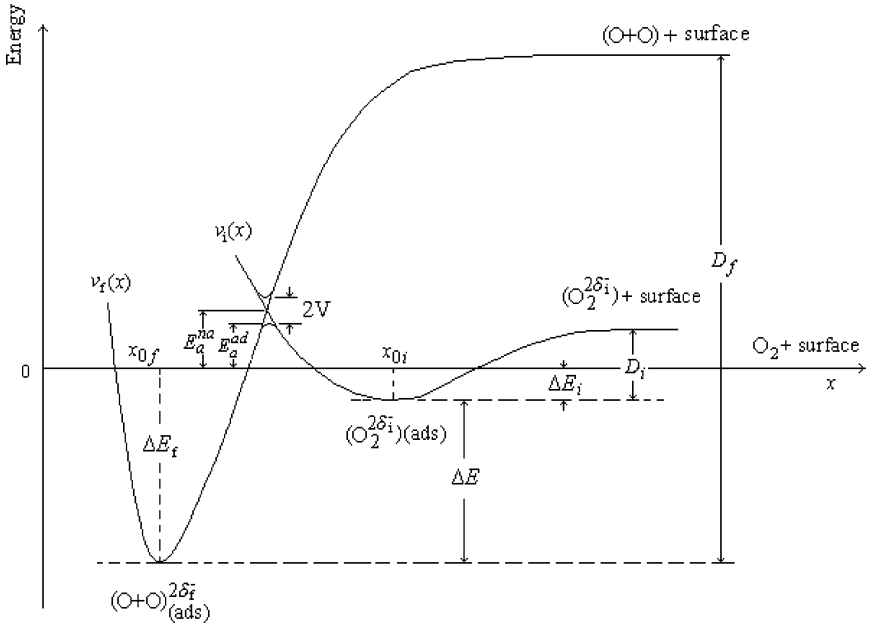

Figure 5. Morse potential energy curves along the *x*-coordinate that illustrate O_2 molecularly adsorbed and dissociative states. x_{0i} and x_{0f} are the initial and the final equilibrium distances of O_2 on a surface. ΔE is the reaction heat, ΔE_i and ΔE_f are the corresponding adsorption heats, and D_i and D_f are the dissociation parameters of the corresponding Morse curves.

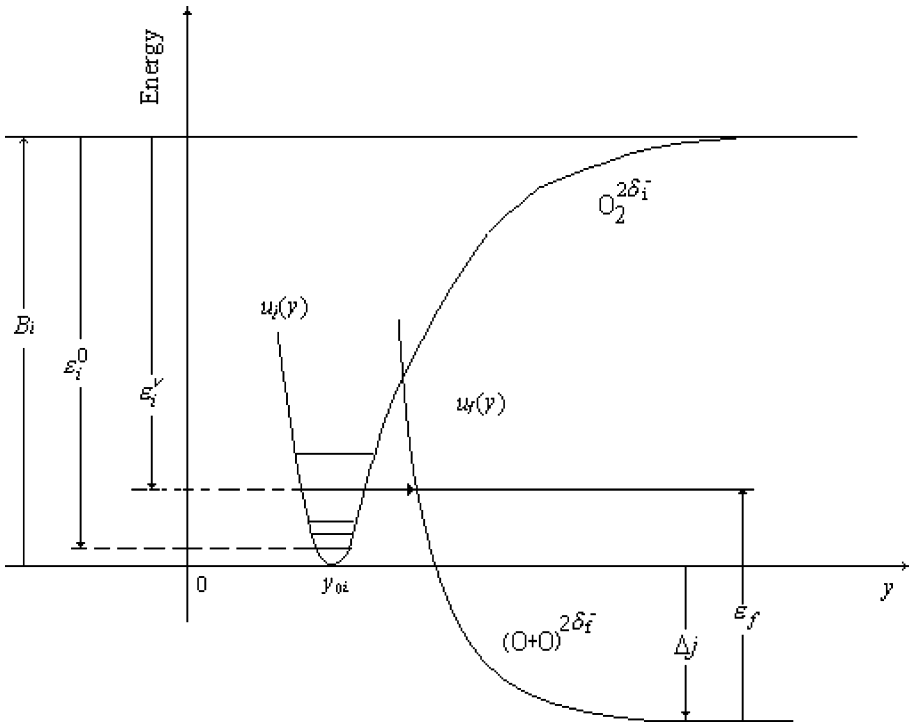

Figure 6. Morse/exponential potentials along the *y*-coordinate describing the molecular adsorbed and dissociated states. B_i is the dissociation parameter of the potential curve u_i, and Δj is the energy of transition along the coordinate *y*.

$$u_i(y) = B_i[1 - e^{-\alpha_i(y-y_{0i})}]^2 \quad \text{(C4)}$$

where

$$\alpha_i = \omega_i^y \sqrt{\mu/2B_i} \quad \text{(C5)}$$

In eq C5, μ is the reduced mass of the O−O vibration and ω_i^y is the corresponding frequency. The repulsive interaction between the dissociated oxygen atoms is described according to refs 20 and 21 by the exponential function (Figure 6)

$$u_f(y) = B_f^e e^{-2\alpha_f(y-y_{0i})} \quad \text{(C6)}$$

with the parameters B_f^e and α_f. The dissociation energies of the Morse potentials, $v_i(x)$ and $v_f(x)$, depend on the adsorption heats ΔE_i and ΔE_f by eqs C7 and C8[21]

$$D_i = |\Delta E_i| + EA_{O_2}^{adiab} \quad \text{(C7)}$$

$$D_f = D(O_2) + |\Delta E_f| \quad \text{(C8)}$$

where $D(O_2)$ is the dissociation energy and $EA_{O_2}^{adiab}$ is the

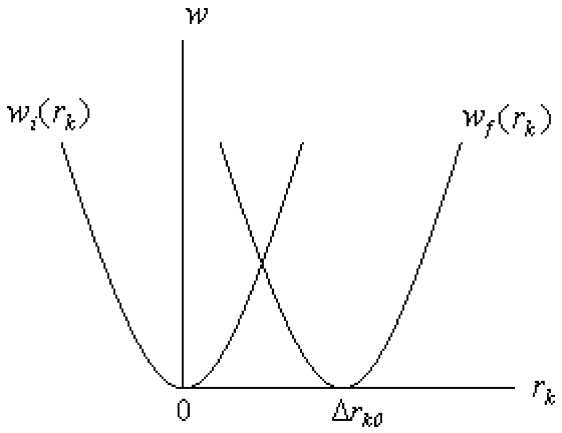

Figure 7. Potential energy curves along the metal coordinate r_k.

adiabatic electron affinity of the oxygen molecule. Following ref 21, we take the dissociation energy for the potential $u_i(y)$, $B_i = 80$ kcal/mol, and the dissociation energy for the potential $u_f(y)$, $B_f^e = 0.3B_i$.

The potential energies $w_i(\{r_k\})$ and $w_f(\{r_k\})$ for metal atom vibrations are usually written in harmonic approximation (Figure 7) since metal atoms perform small vibrations in the crystal lattice; these potential energies are represented as the sum of the harmonic potentials of a set of independent oscillators

$$w_i(\{r_k\}) = {}^1/_2 \sum_k m\omega_k{}^2 r_k{}^2 \qquad \text{(C9)}$$

$$w_f(\{r_k\}) = {}^1/_2 \sum_k m\omega_k{}^2 (r_k - \Delta r_{k0})^2 \qquad \text{(C10)}$$

where the r_k values are the metal atom coordinates, $\Delta r_{k0} = r_{k0f} - r_{k0i}$, ω_k values are the vibration frequencies, and m values are the reduced masses.

The effective electron resonance integral V (that mixes the states with a nondissociated and dissociated X_2 molecule) depends in general on the distance between the adsorbate molecule and the surface, x, on the distance X···X, y, and on displacements of substrate atoms r_k. The dependence of V on r_k is usually assumed to be weak.[20,25,36] So, we shall approximately suppose the resonance integral V to be dependent on x- and y-coordinates only.

The constant V_0 and the parameter ϵ in the equation for the electron resonance integral

$$V = V_0 e^{-(x-x_{0f})/a_x}(1 - \epsilon e^{-(y-y_{0i})/a_y}) \qquad \text{(C11)}$$

should come from quantum chemical and molecular dynamics calculations and should be given reasonable and hopefully realistic values. Here we take the value of $V_0 = 3$ kcal/mol and $a_x = a_y = 1$ Å that are close to the value accepted in the paper[36] and $\epsilon = 0.3$.

D. Reorganization Energy. The reorganization energy was estimated using the difference Δr of the bond lengths M−M of the metal cluster (Figure 4) interacting with the molecular oxygen and with oxygen atoms by the equation

$$E_r = (1/2)Nm\Omega^2\Delta r^2 \qquad \text{(D1)}$$

where N is the number of metal−metal bonds of the model metal cluster and m is the reduced mass of the metal−metal vibration equal to half of the metal atom mass. The frequency Ω in eq D1 characterizes collective vibrations of lattice atoms, and its value might be extracted from the spectrum of the frequency dependence of the complex dielectric function of the solid as discussed in more detail in ref 19. Following this reference, we have taken this frequency to be equal to $\sim k_B T/\hbar = 210$ cm^{-1}.

Acknowledgment. The work supported by the Israel Science Foundation. The authors thank Dr. I. Efremenko for useful discussions.

References and Notes

(1) Evans, M. G.; Polanyi, M. *Trans. Faraday Soc.* **1938**, *34*, 11.
(2) Brønsted, J. N.; Pedersen, K. J. *Z. Phys. Chem.* **1924**, *108*, 185. Brønsted, J. N. *Chem. Rev.* **1928**, *5*, 231.
(3) Horiuti, J.; Polanyi, M. *Acta Physicochim.* **1935**, *2*, 505.
(4) Bell, R. P. *Proc. R. Soc. London, Ser. A* **1936**, *154*, 414.
(5) Bell, R. P. *The Proton in Chemistry*; Chapman & Hall: London, 1973.
(6) Semenov, N. N. *Some Problems in Chemical Kinetics and Reactivity*; Princeton University Press: Princeton, NJ, 1958.
(7) Nørskov, J. K.; Bligaard, T.; Logadottir, A.; Bahn, S.; Hansen, L. B.; Bollinger, M.; Bengaard, H.; Hammer, B.; Sljivancanin, Z.; Mavrikakis, M.; Xu, Y.; Dahl, S.; Jacobsen, C. J. H. *J. Catal.* **2002**, *209*, 275.
(8) Logadottir, A.; Rod, T. H.; Nørskov, J. K.; Hammer, B.; Dahl, S.; Jacobsen, C. J. H. *J. Catal.* **2001**, *197*, 229.
(9) Bligaard, T.; Nørskov, J. K.; Dahl, S.; Matthiesen, J.; Christensen, C. H.; Sehested, J. S. *J. Catal.* **2004**, *224*, 206.
(10) Bligaard, T.; Honkala, K.; Logadottir, A.; and Nørskov, J. K. *J. Phys. Chem. B* **2003**, *107*, 9325.
(11) Agmon, N. *Int. J. Chem. Kinet.* **1981**, *13*, 333.
(12) Sutin, N. *Acc. Chem. Res.* **1982**, *15*, 275.
(13) Eberson, L. *Electron transfer in Organic Chemistry*; Springer-Verlag: Heidelberg, Germany, 1987.
(14) Lund, H.; Daasbjertg, K.; Lund, T.; Peredsen, S. U. *Acc. Chem. Res.* **1995**, *28*, 313.
(15) Ramirez-Corredores, M. M.; Machin, I.; Grillo, M. E. *J. Mol. Catal. A* **2000**, *151*, 271.
(16) Parsons, R. *Top. Pure Appl. Electrochem.* **1975**, 91.
(17) Isao, M.; Yukio, Y. *J. Catal.* **1967**, *9*, 57.
(18) German, E. D.; Efremenko, I.; Kuznetsov A. M.; Sheintuch, M. *J. Phys. Chem. B.* **2002**, *106*, 11784.
(19) German, E. D.; Kuznetsov, A. M. *J. Mol. Struct. THEOCHEM* **2004**, *671*, 153.
(20) German, E. D.; Kuznetsov, A. M.; Sheintuch, M. *Surf. Sci.* **2004**, *554*, 159.
(21) German, E. D.; Kuznetsov, A. M.; Sheintuch, M. *Surf. Sci.* **2004**, *554*, 170.
(22) German, E. D.; Efremenko, I. *J. Mol. Struct. THEOCHEM* **2004**, *711*, 1.
(23) German, E. D.; Kuznetsov A. M.; Sheintuch, M. *J. Phys. Chem. A* **2005,** *109*, 3542.
(24) Nolan, P. D.; Wheeler, M. C.; Davis, J. E.; Mullins, C. B. *Acc. Chem. Res.* **1998**, *31*, 798.
(25) Kuznetsov, A. M. *Charge transfer in Physics, Chemistry and Biology*; Gordon & Breach: Reading, U.K., 1995.
(26) German, E. D. *Chem. Phys.* Special Issue: Molecular Charge Transfer in Condensed Media, 2005.
(27) Eichler, A. G.; Mittendorfen, F.; Hafner, J. *Phys. Rev. B* **2000**, *62*, 4744.
(28) Frisch, M. J.; Trucks, G. W.; Schlegel, H. B.; Scuseria, G. E.; Robb, M. A.; Cheeseman, J. R.; Zakrzewski, V. G.; Montgomery, Jr. J. A.; Stratmann, R. E.; Burant, J. C.; Dapprich, S.; Millam, J. M.; Daniels, A. D.; Kudin, K. N.; Strain, M. C.; Farkas, O.; Tomasi, J.; Barone, V.; Cossi, M.; Cammi, R.; Mennucci, B.; Pomelli, C.; Adamo, C.; Clifford, S.; Ochterski, J.; Petersson, G. A.; Ayala, P. Y.; Cui, Q.; Morokuma, K.; Rega, N.; Salvador, P.; Dannenberg, J. J.; Malick, D. K.; Rabuck, A. D.; Raghavachari, K.; Foresman, J. B.; Cioslowski, J.; Ortiz, J. V.; Baboul, A. G.; Stefanov, B. B.; Liu, G.; Liashenko, A.; Piskorz, P.; Komaromi, I.; Gomperts, R.; Martin, R. L.; Fox, D. J.; Keith, T.; Al-Laham, M. A.; Peng, C. Y.; Nanayakkara, A.; Challacombe, M.; Gill P. M. W.; Johnson, B.; Chen, W.; Wong, M. W.; Andres, J. L.; Gonzalez, C.; Head-Gordon, M.; Replogle, E. S.; and Pople J. A. *Gaussian 98, Revision A.11.3*; Gaussian, Inc.: Pittsburgh, PA, 2002.
(29) Becke, A. D. *J. Chem. Phys.* **1993**, *98*, 5648
(30) Lee, C.; Yang, W.; Parr, R. G. *Phys. Rev. B* **1998,** *37*, 785.
(31) Hay, P. J.; Wadt, W. R. *J. Chem. Phys.* **1985**, *82*, 299.
(32) Valerio, G.; Toulhoat, H. *J. Phys. Chem.* **1996**, *100*, 10827.
(33) Zacarias, A. G.; Castro, M.; Tour J. M.; Seminario, J. M. *J. Phys. Chem. A* **1999,** *103*, 7692.
(34) Efremenko, I.; German, E. D.; Sheintuch, M. *J. Phys. Chem. A* **2000**, *104*, 8089.

(35) Woon, D. E.; Dunning, T. H., Jr. *J. Chem. Phys.* **1993**, *98*, 1358.
(36) Koper, M. T. M.; Voth, G. A. *J. Chem. Phys.* **1998**, *109*, 1991.
(37) Guo, X.; Hoffman, A.; Yates, J. T. *J. Chem. Phys*. **1989**, *90*, 5787.
(38) Conrad, H.; Ertl, G.; Kupers, J.; Latta, E. *Surf. Sci.* **1977**, *65*, 245.
(39) Imbihl, R.; Demutz, J. E. *Surf. Sci.* **1986**, *173*, 395.
(40) Kolasinski, K. W.; Cemic, F.; Hassebrink, E. *Chem. Phys. Lett*. **1994**, *219*, 113
(41) Nolan, P. D.; Lutz, B. P.; Tanaka, P. L.; Mullins, C. B. *Surf. Sci*. **1998**, *419*, L107.
(42) Honkala, K.; Laassonen, K. *J. Chem. Phys.* **2001**, *115*, 2297.
(43) Eichler, A. G.; Hafner, J. *Phys. Rev. Lett.* **1997**, *79*, 4481.
(44) Pedio, M.; Becker, L.; Hillert, B.; D′Addato, S.; Haase, J. *Phys. Rev. B* **1990**, *41*, 7462.
(45) Schmidtke, E.; Schwennicke, C.; Pfnur, H. *Surf. Sci.* **1994,** *312*, 301.
(46) Stuckless, J. T.; Wartnaby, C. E.; Al-Sarraf, N.; Dixon-Warren, St. J. B.; Kovar, M.; King, D. A. *J. Chem. Phys.* **1997**, *106*, 2012.
(47) Mendez, M. A.; Oed, W.; Fricke, A.; Hammer, L.; Heinz, K.; Muller, K. *Surf. Sci.* **1991**, *253*, 99.
(48) Marcus, P. M.; Demuth, J. E.; Jepsen, D. W. *Surf. Sci.* **1975**, *53*, 501.
(49) Yamagishi, S.; Jenkins, S. J.; King, D. A. *Surf. Sci*. **2003**, *543*, 12.
(50) Gland, J. L.; Sexton, B.; Fisher, G. B. *Surf. Sci.* **1980**, *95*, 587.
(51) Gland, J. L. *Surf. Sci.* **1980**, *93*, 487.
(52) Winkler, A.; Guo, X.; Siddiqui, H. R.; Hagans, P. L.; Yates, J. T. *Surf. Sci*. **1988**, *201*, 419.
(53) Steininger, H.; Lehwald, S.; Ibach, H. *Surf. Sci.* **1982**, *123*, 1.
(54) Lehwald, S.; Ibach, H.; Steiniger, H. *Surf. Sci.* **1982**, *117*, 342.
(55) Starke, U.; Materer, N.; Barbieri, A.; Doll, R.; Heintz, K.; van Hove, M. A.; Somorjai, G. A. *Surf. Sci.* **1993**, *287/288*, 432.
(56) Yeo, Y. Y.; Vattuone, L. King, D. A. *J. Chem. Phys.* **1997**, *106*, 392.
(57) Outka, D. A.; Stohr, J.; Jark, W.; Stevens, P.; Solomon, J.; Madix, R. J. *Phys. Rev. B* **1987**, *35*, 4119.
(58) Parker, D. H.; Bartram, M. E.; Koel, B. E. *Surf. Sci.* **1989**, *217*, 489.
(59) Wurth, W.; Stohr, J.; Feulner, P. Pan, X.; Bauchspiese, K. R.; Baba, Y.; Hundel, E.; Rocker, G.; Meuzel, D. *Phys. Rev. Lett.* **1990**, *65*, 2426.
(60) Campbell, C. T.; Ertl, G.; Kuipers, H.; Segner, J. *Surf. Sci.* **1981**, *107*, 220.
(61) Puglia, C.; Nilsson, A.; Hernnas, B.; Karis, O.; Bennich, P.; Martensson, N. *Surf. Sci.* **1995**, *342*, 119.
(62) Zhu, X. Y.; Hatch, S. R.; White, J. M. *J. Chem. Phys.* **1989**, *91*, 5011.
(63) Jacob, T.; Muller, R. P.; Goddard, W. A., III *J. Phys. Chem. B* **2003**, *107*, 9465.
(64) Li, T.; Balbuena, P. *J. Phys. Chem. B* **2001**, *105*, 9943.
(65) Sueyoshi, T.; Sasaki, T.; Iwasawa, Y. *Surf. Sci.* **1996**, *365*, 310.
(66) Haase, J.; Kuhr, H. J. *Surf. Sci*. **1988**, *203*, L695.
(67) Habraken, F. H. P.; Kieffer, E. Ph.; Bootsma, G. A. *Surf. Sci*. **1979**, *83*, 45.
(68) Dubois, L. H. *Surf. Sci.* **1982**, *119*, 399.
(69) Giamello, E.; Fubini, B.; Lauro, P.; Bossi, A. *J. Catal.* **1984**, *87*, 443.
(70) Jiang, L,; Wang, J.; Cai, Z.; Pan, Y.; Zhao, X. *J. Mol. Struct. THEOCHEM* **2004**, *710*, 97.
(71) Wang, Z. X.; Tlan, F. H. *J. Phys. Chem. B* **2003**, *107*, 6153.
(72) Xu, Y.; Mavrikakis M. *Surf. Sci*. **2001**, *494*, 131; **2003**, *538*, 219.
(73) Koper, M. T.; van Santen, R. A. *J. Electroanal. Chem.* **1999**, *472*, 126.
(74) Cornish, J. C. L.; Avery, N. R. *Surf. Sci.* **1990**, *235*, 209.
(75) Davis, J. E.; Nolan, P. D.; Karseboom, S. G.; Mullins, C. B. *J. Chem. Phys.* **1997**, *107*, 943.
(76) Ivanov, V. P.; Boreskov, G. K.; Savchenko, V. J.; Egelhoff, W. F.; Weinberg, W. H. *Surf. Sci*. **1976**, *61*, 207.
(77) Xu, Y.; Mavrikakis, M. *J. Chem. Phys.* **2002**, *116*, 10846.
(78) Madey, T. K.; Engelhardt, M. A.; Menzel, D. *Surf. Sci*. **1975**, *48*, 304.
(79) Savelieva, G. A.; Speranskaya, G. V.; Popova, N. M. *React. Kinet. Catal. Lett.* **1980**, *13*, 12.